Supporting Information

Enhanced thermal conductivity in oriented polyvinyl alcohol/graphene oxide composites

Xinglong Pan,[a] Michael G. Debije, Albert, P. H. J. Schenning,[a,b,□] Cees W. M. Bastiaansen,[a,c,□]

a. Laboratory of Stimuli-responsive Functional Materials & Devices (SFD), Department of Chemical Engineering and Chemistry, Eindhoven University of Technology, Den Dolech 2, 5612 AZ, Eindhoven, The Netherlands

b. Institute for Complex Molecular Systems, Eindhoven University of Technology, Den Dolech 2, 5612 AZ, Eindhoven, The Netherlands

c. School of Engineering and Materials Science, Queen Mary, University of London, London E1 4NS, United Kingdom

E-mail: a.p.h.j.schenning@tue.nl, c.w.m.bastiaansen@tue.nl

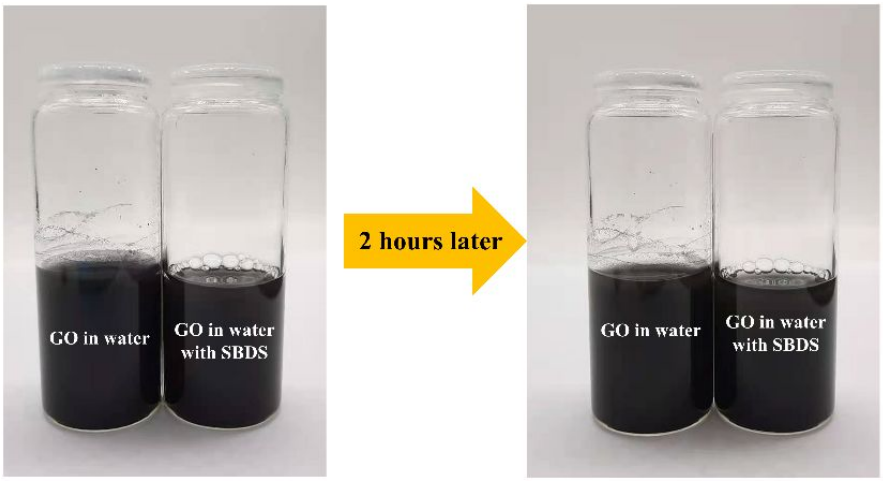

Figure S1. GO and GO/SDBS dispersions in water (GO/water: 0.4 mg/mL) immediately and two hours after ultrasonication for 1 hour and then manual shaking twice. There is no obvious sediment of two dispersion after 2 hours, indicating that there is no obvious improved stability of GO after adding SDBS.

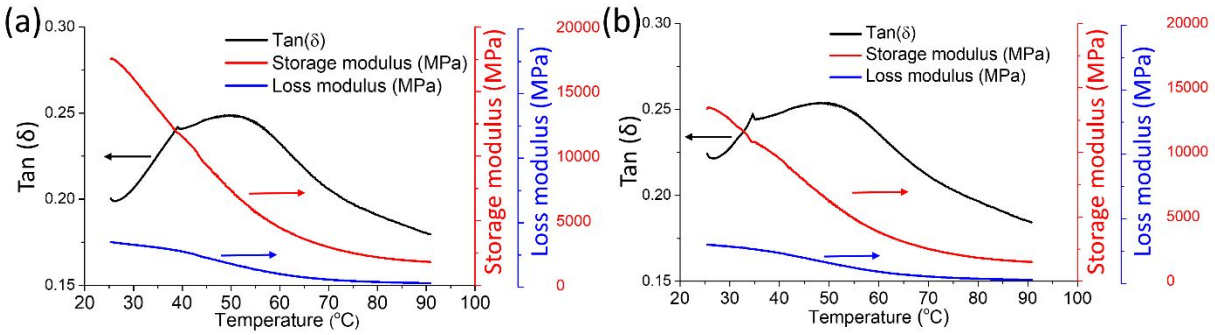

Figure S2. DMA of (a) drawn PVA-5 without SDBS (PVA-5(2)) and (b) drawn PVA-5 with 5 wt% SDBS (PVA-5(3)).

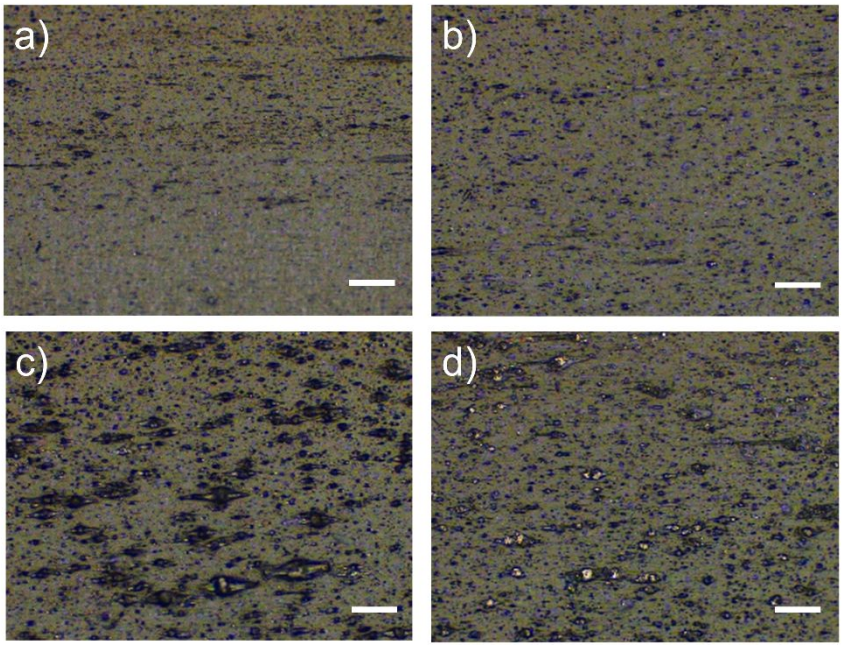

Figure S3. Optical microscopy images of drawn PVA-5(2) (a,c) and PVA-5 (b,d) films. Here, a and b are the top surfaces while c and d are the bottom surfaces of the drawn films. The scale bar is 50 μm.

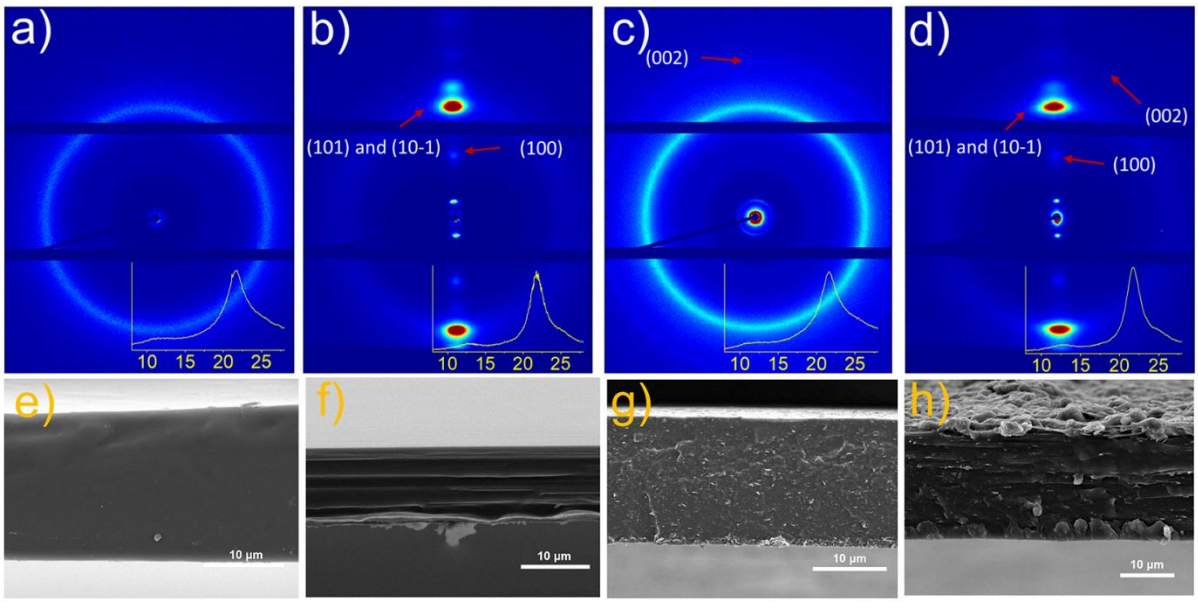

Figure S4. Wide-angle X-ray scattering (WAXS) patterns of undrawn and drawn PVA-0 (a, b), undrawn and drawn PVA-5 composite films (c, d), respectively. The insets are the 1-D curves of X-ray scattering. e-h) SEM images of the cross-section of undrawn and drawn PVA-0 (e, f), undrawn and drawn PVA-5 composite films (g, h), respectively.

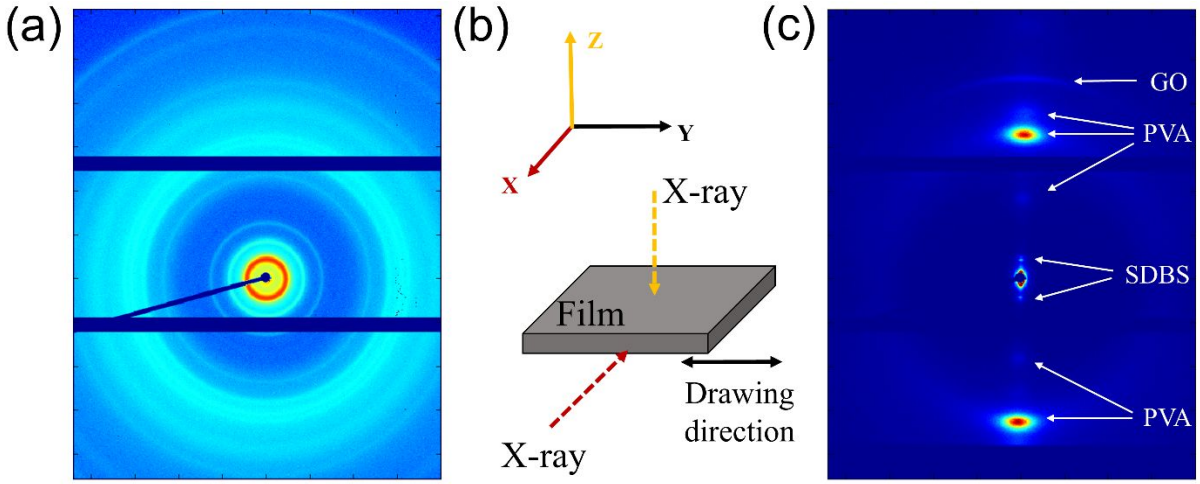

Figure S5. (a) WAXS of SDBS powder. The main peak of SDBS is at 2Θ ~ 3.1 °. In combination with Figure 3d and Figure S2d, this indicates that the SDBS is also oriented in drawn PVA-5 films. (b) Schematic diagram of incident X-ray in WAXS measurement. In Figure 3 and Figure S4, the incident X-ray (the yellow arrow) is perpendicular to the plane of the films. (c) WAXS of drawn PVA-5 film. The incident X-ray (the red arrow in Figure S5b) is parallel to the plane of drawn PVA-5 film, which indicating the anisotropic GO in the plane of drawn PVA-5 films.

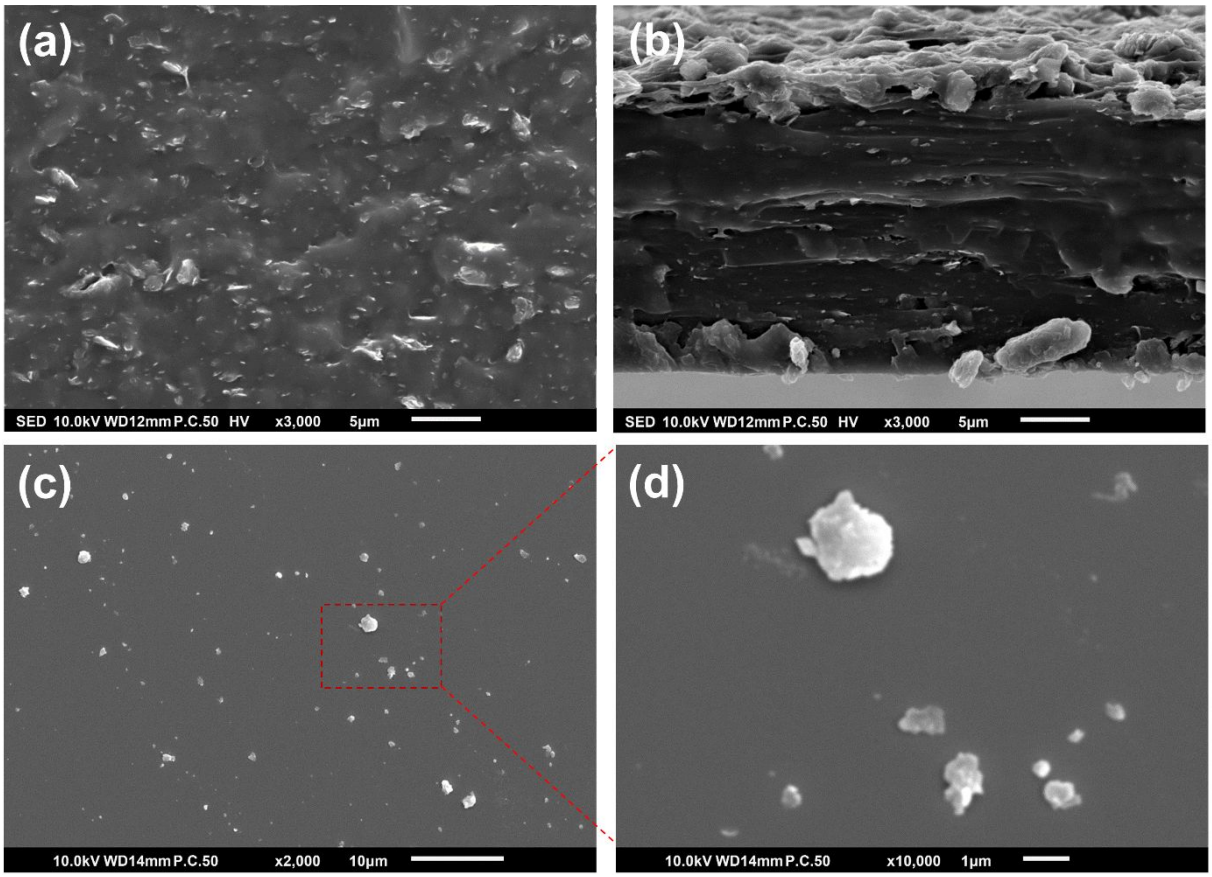

Figure S6. SEM images of the cross-section of undrawn (a) and drawn (b) PVA/GO films with a high resolution. SEM images of GO (c and d). Here, d is the zoom-in graph of the indicated region in c.

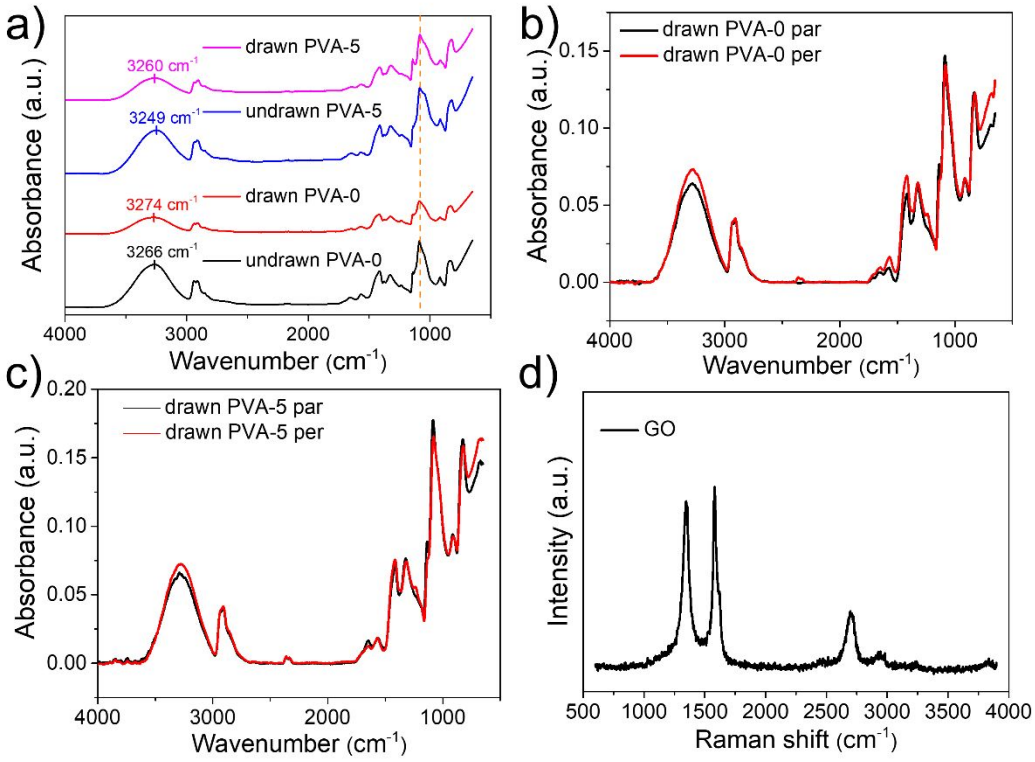

Figure S7. a) Non-polarized FTIR spectra of PVA-0 and PVA-5 films. The orange dashed line indicates there is no obvious shift in spectral position at the peak position of C-O groups. b) and c) Normalized polarized FTIR spectra of PVA films and PVA composite films measured parallel and perpendicular to the drawing direction. Here, the peak of -CH_2 at ~ 2930 cm^{-1} is used as the reference. d) Raman spectrum of GO powder exhibiting absorption peaks at 1350 cm^{-1}, 1580 cm^{-1}, 1620 cm^{-1}, and 2700 cm^{-1}, referred to as D, G, D', and G' (2D) peaks, while the D and G peaks are attributed by the defects and crystallinity in GO, respectively.[1,2] Thus, the intensity ratio of D and G peaks can be used to describe the disorder of groups in GO. The intensity of the D' peak at ~1620 cm^{-1} represents the defects on the edge of GO, indicating the presence of oxidization groups in GO powder.

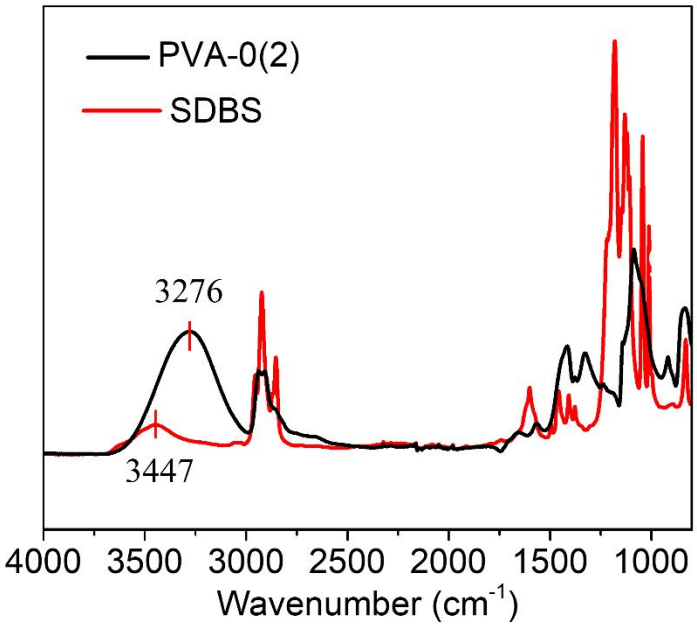

Figure S8. Non-polarized FTIR spectra of SDBS powder and an undrawn PVA-0(2) film.

Table S1 Thermal conductivities of composite films in the literature.[3-15]

	Samples	Contents of thermal-conductive additives (wt%)	Thermal conductivity (W m^{-1} K^{-1})
1	PVA	0	0.3-0.5
2	PVA/cellulose	0	1.2
3	Drawn PVA	0	8.51
4	Drawn PE	0	62-65
5	Drawn PE/GN	0.1	75
6	PE/GO	1	0.36
7	Cellulose/RGO	1	12.6
8	Rubber/CNT/GO	3	0.45
9	PE/GO	5	0.65
10	PVA/GO (this work)	5	25
11	PVDF/CNT/GO	10	0.9
12	Drawn PE/GN	10	5.9
13	PVA/GN	10	13.8
14	PP/GN	12	1.6
15	PE/GN	20	4.5
16	PE/GT/CNT	22	3
17	Epoxy/GN	25	12
18	Cellulose/RGO	30	6

Table S2 Mechanical properties of drawn PVA-5 films without and with 5 wt% SDBS.

Films	**PVA-5 without SDBS**			**PVA-5 with 5 wt% SDBS**		
3 samples in each film	1	2	3	1	2	3
Draw ratio$_{max}$(λ_m)	5.0	5.1	5.5	6.0	5.6	5.8
Average λ_m	5.2			5.8		
Young's modulus (GPa)	~ 25.4			~ 15.9		

References

(1) Kudin, K. N.; Ozbas, B.; Schniepp, H. C.; Prud'homme, R. K.; Aksay, I. A.; Car, R. Raman Spectra of Graphite Oxide and Functionalized Graphene Sheets. *Nano Lett* **2008**, *8*, 36.

(2) Claramunt, S.; Varea, A.; López-Díaz, D.; Velázquez, M. M.; Cornet, A.; Cirera, A. The Importance of Interbands on the Interpretation of the Raman Spectrum of Graphene Oxide. *J Phys Chem C* **2015**, *119*, 10123.

(3) Pan, X.; Shen, L.; Schenning, A. P. H. J.; Bastiaansen, C. W. M. Transparent, High-Thermal-Conductivity Ultradrawn Polyethylene/Graphene Nanocomposite Films. *Adv Mater* **2019**, *31*, 1904348.

(4) Shrestha, R.; Li, P.; Chatterjee, B.; Zheng, T.; Wu, X.; Liu, Z.; Luo, T.; Choi, S.; Hippalgaonkar, K.; De Boer, M. P.; Shen, S. Crystalline Polymer Nanofibers with Ultra-High Strength and Thermal Conductivity. *Nat Commun* **2018**, *9*, 1664.

(5) Park, Y.; You, M.; Shin, J.; Ha, S.; Kim, D.; Heo, M. H.; Nah, J.; Kim, Y. A.; Seol, J. H. Thermal Conductivity Enhancement in Electrospun Poly(Vinyl Alcohol) and Poly(Vinyl Alcohol)/Cellulose Nanocrystal Composite Nanofibers. *Sci Rep* **2019**, *9*, 3026.

(6) Zhuang, Y.; Zheng, K.; Cao, X.; Fan, Q.; Ye, G.; Lu, J.; Zhang, J.; Ma, Y. Flexible Graphene Nanocomposites with Simultaneous Highly Anisotropic Thermal and Electrical Conductivities Prepared by Engineered Graphene with Flat Morphology. *ACS Nano* **2020**, *14*, 11733.

(7) Pan, X.; Schenning, A. H. P. J.; Shen, L.; Bastiaansen, C. W. M. The Role of Polyethylene Wax on the Thermal Conductivity of Transparent Ultradrawn Polyethylene Films. *Macromolecules* **2020**, *53*, 5599.

(8) Xie, X.; Li, D.; Tsai, T.; Liu, J.; Braun, P. V; Cahill, D. G. Thermal Conductivity, Heat Capacity, and Elastic Constants of Water-Soluble Polymers and Polymer Blends. *Macromolecules* **2016**, *49*, 972–978.

(9) Yano, T.; Higaki, Y.; Tao, D.; Murakami, D.; Kobayashi, M.; Ohta, N.; Koike, J. I.; Horigome, M.; Masunaga, H.; Ogawa, H.; Takahara, A. Orientation of Poly(Vinyl Alcohol) Nanofiber and Crystallites in Non-Woven Electrospun Nanofiber Mats under Uniaxial Stretching. *Polymer* **2012**, *53*, 4702.

(10) Kongkhlang, T.; Tashiro, K.; Kotaki, M.; Chirachanchai, S. Electrospinning as a New Technique to Control the Crystal Morphology and Molecular Orientation of Polyoxymethylene Nanofibers. *J Am Chem Soc* **2008**, *130*, 15460.

(11) Tarani, E.; Terzopoulou, Z.; Bikiaris, D. N.; Kyratsi, T.; Chrissafis, K.; Vourlias, G. Thermal Conductivity and Degradation Behavior of HDPE/Graphene Nanocomposites: Pyrolysis, Kinetics and Mechanism. *J Therm Anal Calorim* **2017**, *129* (3), 1715–1726.

(12) Gu, J.; Li, N.; Tian, L.; Lv, Z.; Zhang, Q. High Thermal Conductivity Graphite Nanoplatelet/UHMWPE Nanocomposites. *RSC Adv* **2015**, *5* (46), 36334–36339.

(13) Che, J.; Wu, K.; Lin, Y.; Wang, K.; Fu, Q. Largely Improved Thermal Conductivity of HDPE/Expanded Graphite/Carbon Nanotubes Ternary Composites via Filler Network-Network Synergy. *Compos Part A Appl Sci Manuf* **2017**, *99*, 32–40.

(14) Zhang, W. Bin; Zhang, Z. X.; Yang, J. H.; Huang, T.; Zhang, N.; Zheng, X. T.; Wang, Y.; Zhou, Z. W. Largely Enhanced Thermal Conductivity of Poly(Vinylidene Fluoride)/Carbon Nanotube Composites Achieved by Adding Graphene Oxide. *Carbon* **2015**, *90*, 242–254.

(15) Ronca, S.; Igarashi, T.; Forte, G.; Rastogi, S. Metallic-like Thermal Conductivity in a

Lightweight Insulator: Solid-State Processed Ultra High Molecular Weight Polyethylene Tapes and Films. *Polym* **2017**, *123*, 203–210.